

Electronic Supplementary Information (ESI) available for:

Supersaturated spontaneous nucleation to TiO₂ microspheres: Synthesis and giant dielectric performance

5

Wanbiao Hu, Liping Li, Wenming Tong, Guangshe Li*

State Key Laboratory of Structural Chemistry, Fujian Institute of Research on the Structure of Matter and Graduate School of Chinese Academy of Sciences, Fuzhou 350002 (P. R. China)

10

Fax: (+) 86-591-83714946

E-mail: guangshe@fjirsm.ac.cn

Supporting Online Materials

15

S1. XRD patterns of rutile TiO₂ prepared by adjusting the initial concentration (TiCl₄) and reaction temperature.

S2. XRD pattern and SEM images of rutile TiO₂ prepared under hydrothermal conditions: 2.3 M, 120 °C, 2h.

20

S3. XRD patterns and SEM images of rutile TiO₂ prepared by modulating the reaction time under hydrothermal conditions: 2.3 M, 160 °C.

S4. XRD pattern of rutile TiO₂ prepared under hydrothermal conditions: 2.3 M, 160 °C, 2h.

S5. SEM image of chapped hierarchical TiO₂ microsphere.

S6. Structural scheme of rutile TiO₂.

25

S7. Impedance spectrum of as-prepared TiO₂ microspheres measured at room temperature.

Experimental Section

(i) Preparation of rutile TiO₂ hierarchical microspheres

Sample synthesis was performed by a solution chemistry using the following procedure: 22.5 mL TiCl₄ (99%) was added dropwise into 70 mL water at 0 °C in an ice-water bath under vigorously magnetic stirring, which led to 2.3 M TiCl₄ solution. After stirring for 30 min, this solution was moved to an ambient condition while stirring for another 4 h, and then transferred into Teflon-lined stainless steel autoclaves (100 mL). These autoclaves were allowed to react at 160 °C for 2 h. After cooling to room temperature, the precipitate was collected and washed by distilled water to obtain the final products.

Similar preparation procedures were also employed to investigate the impacts of the preparation conditions like reaction time, initial concentration, and temperatures on the products.

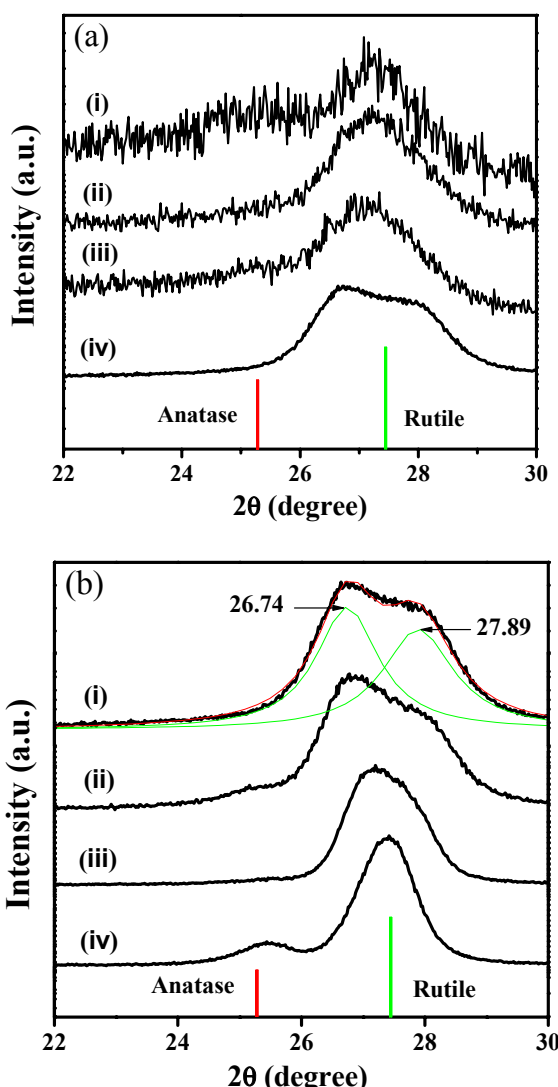
(ii) Sample characterization

Phase purity and crystallinity of the final products were examined by X-ray diffraction (XRD) (Rigaku Dmax2500, Cu K α radiation, $\lambda = 0.15418$ nm). Particle size, morphology, and microstructures were determined by field emission scanning electron microscopy (SEM) (JEOL JSM-6700) and transmission electron microscopy (TEM), selective area electron diffraction (SAED) and high resolution transmission electron microscopy (HRTEM) (JEM-2010).

Dielectric constants of the products were determined by complex impedance measurements in air on compressed pellets of 1.5 mm in thickness and 7.0 mm in diameter. Highly conductive silver paste was painted onto the opposite sides of the pellets and then dried in air at 80 °C for 2 h to form the electrodes. The alternative current (AC) impedance measurements were carried out in a frequency range from 20 Hz to 1 MHz and at an oscillation voltage of 0.5 V using a precision LCR meter (Agilent HP4284A) with an assistant clamp of Agilent 16451B. Impedance data of the samples were

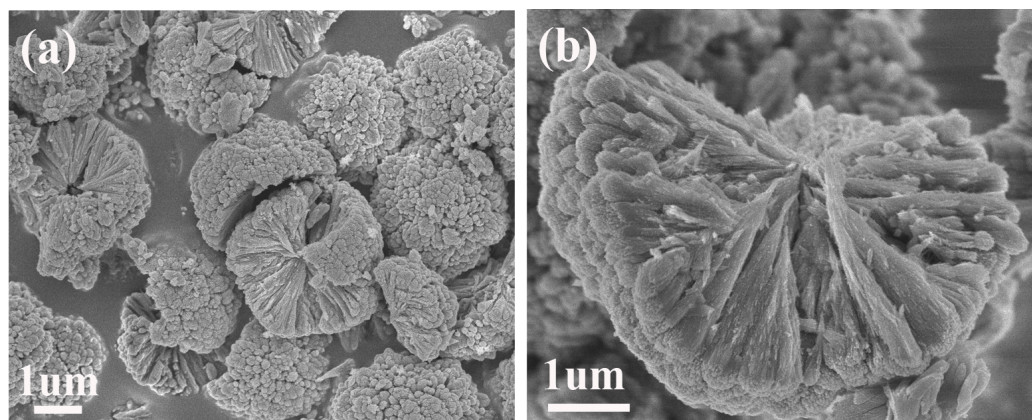
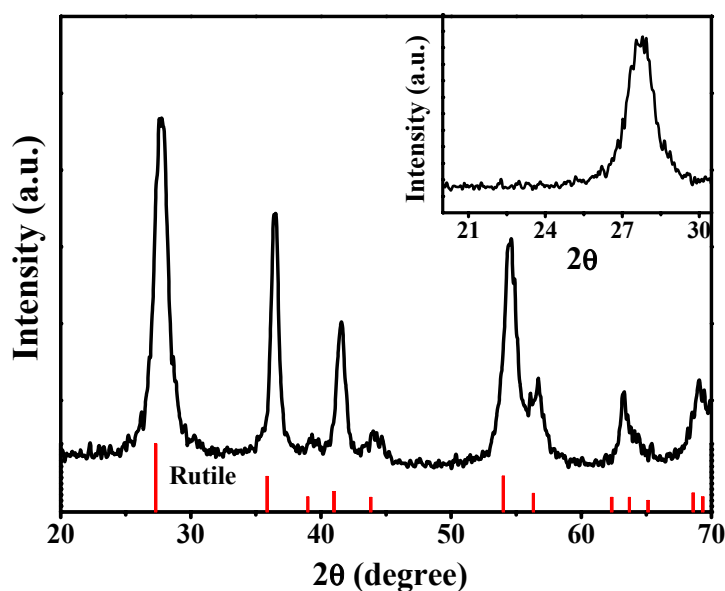
analyzed by an equivalent circuit model using the least-squares refinement program EQUIVCRT for direct determination of the equivalent grain and grain boundary conductivity.

(1) XRD



S1. (a) Enlarged XRD patterns of rutile TiO_2 that was prepared hydrothermally at 120°C for 2h with varying the initial TiCl_4 concentrations: (i) 0.55 M, (ii) 0.75 M, (iii) 1.0 M, and (iv) 1.4 M. (b) Enlarged XRD patterns of rutile TiO_2 prepared by modulating both the initial TiCl_4 concentrations and reaction temperature: (i) 1.4 M, 120°C , (ii) 1.2 M, 120°C , (iii) 1.2 M, 150°C , and (iv) 1.0 M, 150°C . Vertical bars denote the standard diffraction data for anatase (JCPDS, No. 71-1169) and rutile TiO_2 (JCPDS No. 89-4920). Both lines at $2\theta=26.74^\circ$ and 27.89° marked in (b) could not be neither assigned to rutile/anatase, nor brookite (JCPDS No. 29-1360), which implied the presence of uncertain phase. These results indicate that relatively low initial TiCl_4 concentrations or low temperature did not favor the formation of rutile TiO_2 .

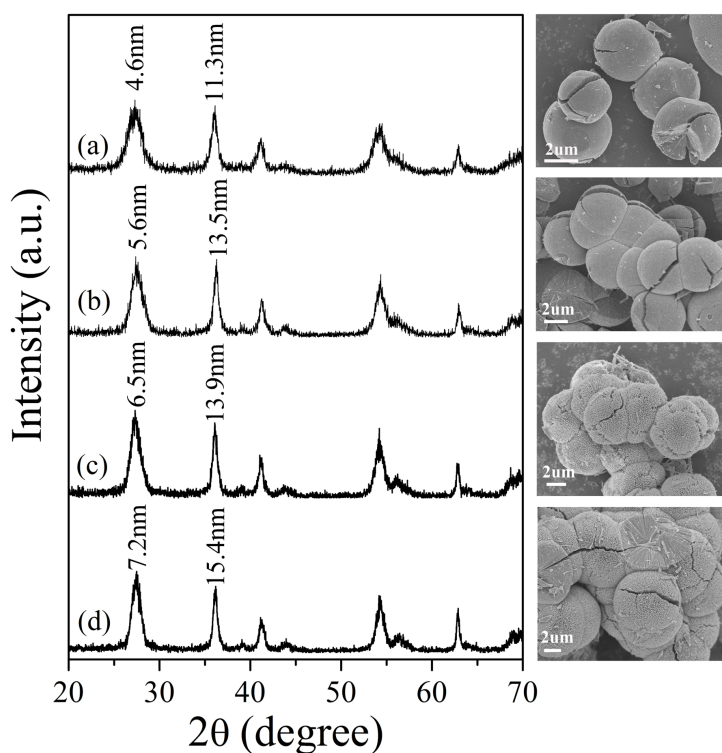
(2) XRD and SEM



5

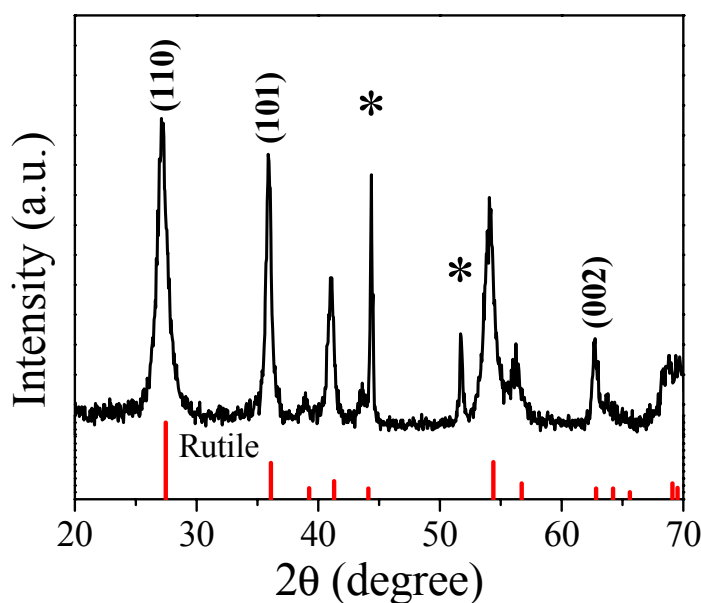
S2. XRD pattern (top) and SEM images (bottom) of rutile TiO_2 that was synthesized by hydrothermal reactions at relatively low temperature of 120°C with an initial TiCl_4 concentration of 2.3 M. Although pure-phase rutile TiO_2 and spherical assembly were obtained, the presence of rough surface and un-uniform bundles indicate that the sample quality of these spherical assemblies is far inferior to that obtained at 160°C .

(3) XRD and SEM



S3. XRD patterns and corresponding SEM images of rutile TiO_2 prepared with initial TiCl_4 concentration of 2.3 M at 160 °C by modulating the reaction time: (a) 25 min, (b) 50 min, (c) 75 min, and (d) 100 min. All the products are pure-phase rutile-typed TiO_2 . When prolonging the aging time from 25 to 100 min, the crystallite size estimated from the strongest line (110) increases from 4.6 to 7.2 nm, while the microsphere dimension extends from 4 μm to 8 μm . Based on the above analysis, it can be concluded that the size estimated using Scherrer formula for line (110) denotes the diameter of single nanowire and that for (101) reflection associates with the length of single nanowire. Therefore, increasing reaction time would result in an increase in crystallite sizes along [100], [010], and [001], namely, *a*-, *b*- and *c*-axis directions respectively. Such a dynamic process belongs to “growth-cum-assembly” as demonstrated in Fig. 1 of the context.

(4) XRD

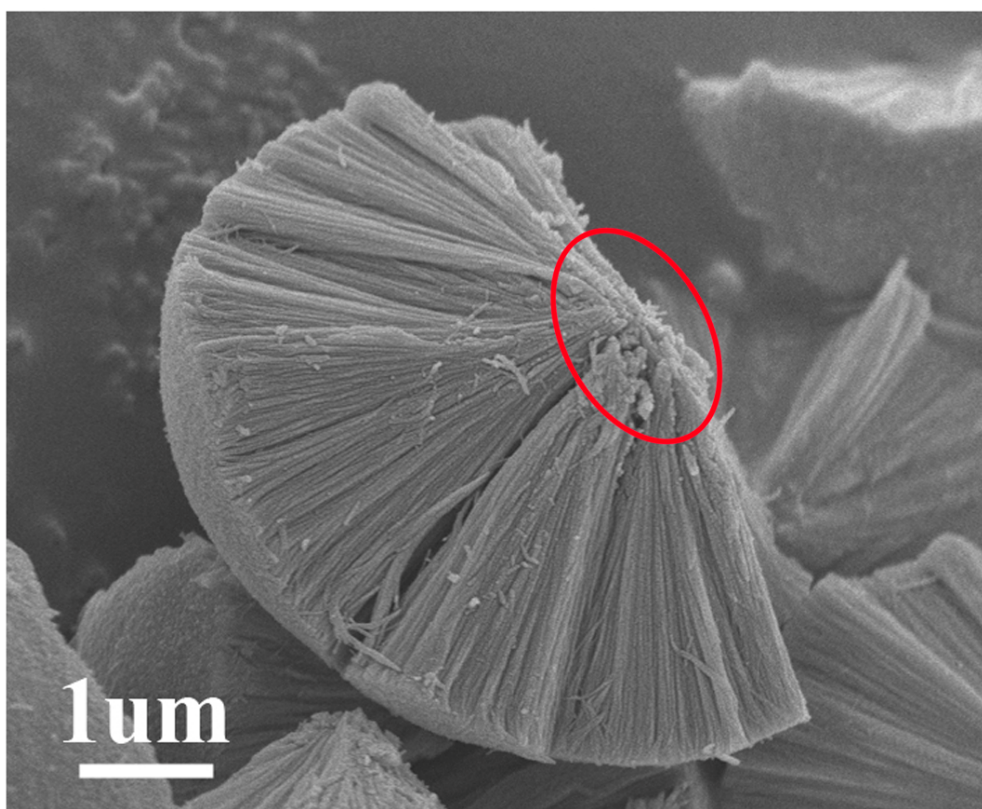


5

S4. XRD pattern of the sample prepared after hydrothermal reaction of 2.3 M TiCl_4 at 160 °C for 2h.

Symbols * denote the internal standard nickel. All diffraction data matched well the vertical bars below the pattern, the standard data for rutile TiO_2 (JCPDS, No. 89-4920), confirming the formation of single phase. The intense diffraction lines like (110) and (101) indicate the high crystallinity. It is also noted that both lines (101) and (002) were significantly narrowed, relative to the line (110), which indicate a preferential orientation of the primary particles.

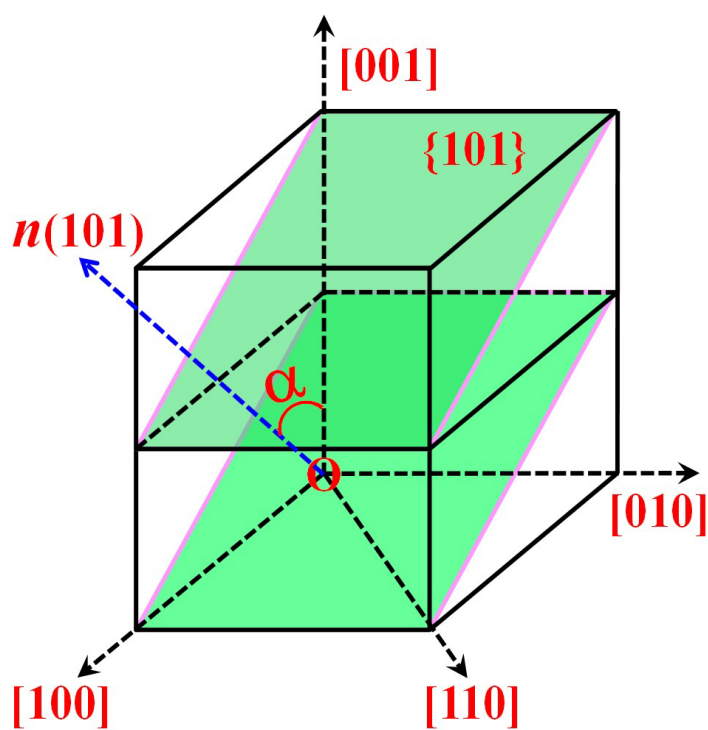
(5) SEM



5

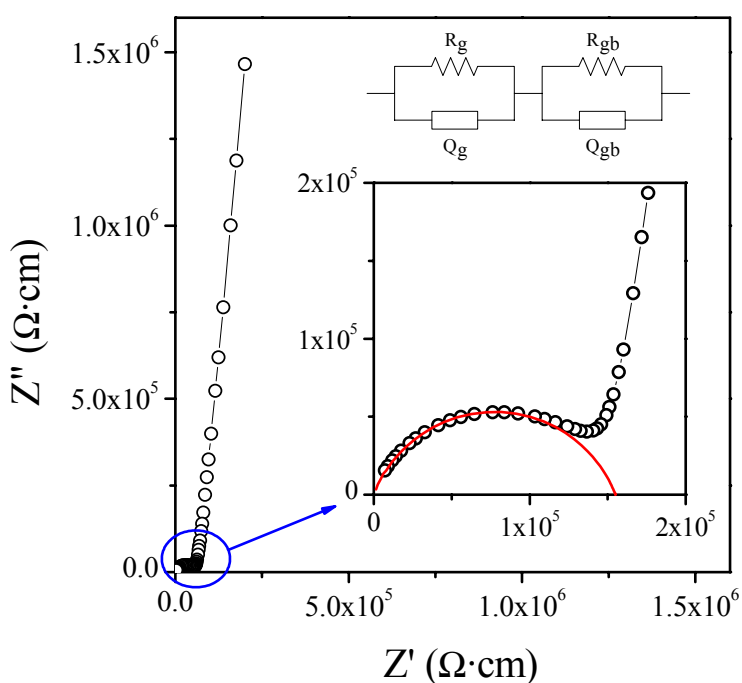
S5. SEM image of a chapped hierarchical microsphere. There exists a center region (highlighted by red ring), from which bundles radiated outwards all directions to produce the hierarchical microspheres.

(6) Structural scheme



S6. Structural scheme of rutile TiO_2 . Here, double lattice cell along c -axis is shown to further illustrate the preferential growth. Various crystal directions denoted in the scheme origin from O-point. Two planes (green) denote the $\{101\}$ facets, and the corresponding normal direction is flagged as $n(101)$ (blue). Angle between $n(101)$ and [001] (or c -axis) is about $\alpha=32.8^\circ$. Obviously, when the growth was along [001] (or c -axis) direction, both diffraction lines (002) and (101) would be narrowed.
Comparatively, owing to the confinement along [110] direction, line (110) would be broadened.

(7) Impedance spectrum



5

S7. Room temperature impedance spectrum of rutile TiO_2 microspheres. The enlarged curve and the equivalent circuit containing a series of resistors R , and constant phase elements Q , are also shown in inset. R_g and R_{gb} represent the grain and grain boundary resistances, and Q_g and Q_{gb} are the corresponding phase elements. Using the equivalent circuit, the impedance data were well fitted (red arc), yielding $R_g=0.1547 \text{ M}\Omega\cdot\text{cm}$, $R_{gb}=14021 \text{ M}\Omega\cdot\text{cm}$, $Q_g=2.27 \text{ nF/cm}$ and $Q_{gb}=20.24 \text{ nF/cm}$. Obviously, R_{gb} is much larger than R_g , which indicates that plenty of carriers were confined within the nanoscale cavities of grain boundaries.